

Dynamics simulation of braiding two Majorana zero modes via a quantum dotLuting Xu,^{*} Jing Bai, Wei Feng, and Xin-Qi Li[†]*Center for Joint Quantum Studies and Department of Physics, School of Science, Tianjin University, Tianjin 300072, China*

(Received 9 April 2023; revised 3 July 2023; accepted 28 August 2023; published 7 September 2023)

In this work we perform real-time simulations for the dynamics of braiding a pair of Majorana zero modes (MZMs) through a quantum dot in a minimal setup of pure one-dimensional realization. We reveal the strong nonadiabatic effect when the dot energy level approaches zero in order to achieve a geometric phase $\pi/4$ which is required for a full exchange between the MZMs. Rather than the strategies of nonuniformly manipulating the system according to adiabatic conditions and shortcuts to adiabaticity, we propose and illustrate a more feasible scheme to suppress the nonadiabatic transition, which allows for a full exchange between the Majorana modes.

DOI: [10.1103/PhysRevB.108.115411](https://doi.org/10.1103/PhysRevB.108.115411)**I. INTRODUCTION**

The nonlocal nature of Majorana zero modes (MZMs) and obeyed non-Abelian exchange statistics provide an elegant paradigm of topological quantum computation (TQC) [1–6]. The exchange (braiding) operations in real space can lead to unitary rotations in the degenerate subspace of ground states, which constitute desired quantum information processing and help realize logic gates in TQC. In the past decade, after great efforts, considerable progress has been achieved for realizing MZMs in various experimental platforms. Yet, the main experimental evidences are associated with the zero-bias conductance peaks, which cannot ultimately confirm the realization of MZMs. A further step in demonstrating the existence of MZMs and the key procedure towards TQC is illustrating the non-Abelian statistics.

Viewing that hybrid semiconductor-superconductor devices, e.g., *s*-wave superconductor proximitized nanowires, have been the leading platform to generate MZMs [7–9], thus an obvious difficulty is that directly exchanging (braiding) the MZMs realized in one-dimensional (1D) nanowires is impossible, since collisions between the MZMs during braiding cannot be avoided in the 1D case. Schemes to combine the 1D wires into a two-dimensional (2D) network (through T or Y junctions) for gate-voltage-controlled moving and exchanging the MZMs have been proposed [10–16], yet progress to resolve the huge technological challenges (necessary controls) is slow. Other proposals of braiding MZMs include tuning local couplings between Majorana modes directly via electric gates [17–20] or indirectly via modulating the role of charging energy on the Majorana islands [21–24] or through quantum dots [25–27], measurement-only schemes [28–31], and others [32].

Very recently, following the braiding protocol via superconducting Y junctions [33–38], an alternative scheme based on more conventional elements, i.e., superconductor

proximitized nanowires connected with a quantum dot (QD), was proposed to braid a pair of MZMs in the 1D case [39], as schematically shown in Fig. 1(a). In the original Y-junction proposal, three Cooper pair boxes are connected at a Y junction via three overlapping Majorana fermions (which effectively produce a single zero mode at the center). This was regarded as the minimal setup required for the braiding of a pair of MZMs, controlled by the fluxes through the three Josephson junctions to a bulk superconductor. In Ref. [39], the setup is simplified to a single 1D Josephson junction, as shown in Fig. 1(a), where two proximitized nanowires are connected through a quantum dot. By tuning the coupling strengths between the MZMs and the QD through gate voltages, the MZMs γ_2 and γ_3 can be exchanged with the help of the QD. In this work we perform real-time simulations for the braiding dynamics of the MZMs in this desired 1D setup.

In particular, we will reveal the strong nonadiabatic effect when the dot energy level approaches zero in order to achieve a geometric phase $\pi/4$, as required for a full exchange between the MZMs. We will also simulate and compare a variety of manipulating schemes, to exploit a proper strategy to suppress the nonadiabatic transition and achieve full exchange between the Majorana modes.

II. BASIC IDEA AND PROBLEM

Let us consider the setup schematically shown in Fig. 1(a), where each topological superconductor wire can be realized by a semiconductor nanowire in proximity contact with an *s*-wave superconductor. For each wire, a pair of MZMs appears at the ends. Here we denote the four MZMs as $\gamma_1, \gamma_2, \gamma_3$, and γ_4 . Actually, using four MZMs is the minimal construction of a Majorana logic qubit in order to conserve the fermion parity (even or odd). For the setup in Fig. 1(a), if combining (γ_1, γ_2) as a regular fermion with occupation $n_{12} = 0$ or 1, and (γ_3, γ_4) as another regular fermion with occupation $n_{34} = 0$ or 1, the four-MZM qubit (with even fermion parity, for example) has logic states $|0_{12}0_{34}\rangle$ and $|1_{12}1_{34}\rangle$. In Fig. 1(a), the QD inserted between the wires is used to mediate exchange between the MZMs γ_2 and γ_3 . If a full exchange is accomplished, i.e.,

^{*}xuluting@tju.edu.cn[†]xinqi.li@tju.edu.cn

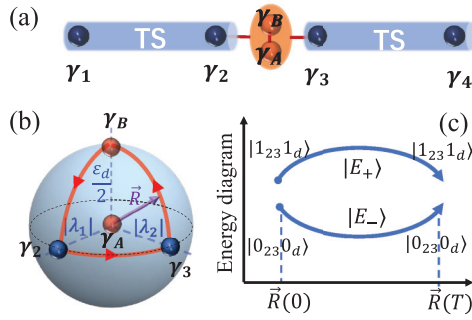


FIG. 1. (a) Schematic diagram for the setup of topological superconductor (TS) nanowires connected with a quantum dot, proposed to braid a pair of MZMs in the 1D case. (b) By splitting the dot electron into a pair of Majorana fermions (γ_A and γ_B), the MZMs γ_2 and γ_3 and the quantum dot can be mapped to a Y junction, which supports formation of a geometric Berry phase, for the use of braiding (exchanging) the Majorana modes γ_2 and γ_3 . (c) Energy diagram of the instantaneous eigenstates $|E_{\pm}\rangle$ in the subspace of even fermion parity. Here, the occupation state $|n_{23}n_d\rangle$ is used, with n_{23} and n_d the occupation numbers of the regular fermions associated with the MZMs γ_2 and γ_3 and the quantum dot, respectively.

$\gamma_2 \rightarrow \gamma_3$ and $\gamma_3 \rightarrow -\gamma_2$ associated with a braiding operator $U = e^{\frac{\Omega}{4}\gamma_2\gamma_3}$, the Majorana qubit state would experience a rotation as

$$|0_{12}0_{34}\rangle \rightarrow |\psi_g\rangle = \frac{1}{\sqrt{2}}(|0_{12}0_{34}\rangle - i|1_{12}1_{34}\rangle), \quad (1)$$

which corresponds to a Hadamard-type logic gate (up to an additional phase shift $\pi/2$).

The QD is assumed to have only a single level involved in the braiding dynamics, with thus a single-level Hamiltonian $H_D = \varepsilon_d d^\dagger d$. The QD is coupled to the MZMs γ_2 and γ_3 , described as $H'_1 = i(\lambda_1 d + \lambda_1^* d^\dagger)\gamma_2$ and $H'_2 = (\lambda_2 d - \lambda_2^* d^\dagger)\gamma_3$. The coupling amplitudes are more explicitly specified as $\lambda_1 = |\lambda_1|e^{i\phi_1/2}$ and $\lambda_2 = |\lambda_2|e^{i\phi_2/2}$, with the phases ϕ_1 and ϕ_2 modulated by controlling the phases of the s -wave superconductors through magnetic fluxes (based on the Aharonov-Bohm effect) as explored in Refs. [40–42]. If we decompose the dot electron into a pair of Majorana fermions γ_A and γ_B , described as $d = (\gamma_B - i\gamma_A)/2$, and modulate the phases as $\phi_1 = \pi$ and $\phi_2 = 0$, we can easily check that γ_B is decoupled with the MZMs γ_2 and γ_3 , and the remaining coupling can be reexpressed as

$$H_M = i\gamma_A(\vec{R} \cdot \vec{\gamma}). \quad (2)$$

Here $\vec{R} = (|\lambda_1|, |\lambda_2|, \varepsilon_d/2)$ and $\vec{\gamma} = (\gamma_2, -\gamma_3, \gamma_B)$ are introduced for the sake of brevity. Satisfactorily, in this way, we have mapped the setup to the configuration of a Y junction [33–38], as shown in Fig. 1(b). Through control of the coupling strengths $|\lambda_1|$ and $|\lambda_2|$ the system can complete a cyclic evolution in the parameter space, which is described by $U = e^{\Omega\gamma_2\gamma_3}$. Here Ω is from the well-known Berry phase, which is half of the solid angle ($\pi/2$, in the case $\varepsilon_d \rightarrow 0$) enclosed by the evolution trajectory in the parameter space. The result $\Omega = \pi/4$ corresponds to a full exchange between γ_2 and γ_3 , and as well the state rotation of the 4-MZMs qubit as mentioned above.

From Fig. 1(b) we know that, in order to precisely realize the solid angle $\pi/2$, we should make $\varepsilon_d \rightarrow 0$. However, this will cause strong nonadiabatic transitions during the initial and final stages of the cyclic evolution, if the speed of evolution is not slow enough. The reason can be understood from the energy diagram depicted in Fig. 1(c), for the instantaneous eigenstates. Here, the occupation state $|n_{23}n_d\rangle$ is used, with n_{23} and n_d the occupation numbers of the regular fermions associated with the MZMs γ_2 and γ_3 and the quantum dot, respectively. Without loss of generality, we only consider the subspace of even fermion parity, i.e., the subspace expanded by the basis states $|0_{23}0_d\rangle$ and $|1_{23}1_d\rangle$. Similar results in the odd-fermion-parity subspace $\{|1_{23}0_d\rangle, |0_{23}1_d\rangle\}$ are briefly analyzed in Appendix A.

We see that, near the beginning and end of the braiding operation, the energy difference of the instantaneous eigenstates $|E_+\rangle$ and $|E_-\rangle$ is ε_d , noting that there is no direct coupling between γ_2 and γ_3 . This near-zero energy gap (when $\varepsilon_d \rightarrow 0$) will make the two-state system suffer strong nonadiabatic transition, unless the evolution is infinitely slow. In this work we would like to investigate the nonadiabatic effect caused by the small ε_d . In particular, we will explore strategies to suppress the nonadiabatic transitions and compare the results of different schemes, including four-step uniform and nonuniform manipulations of the coupling parameters, and an improved six-step manipulating scheme.

III. FOUR-STEP UNIFORM AND NONUNIFORM SCHEMES

Let us start with the four-step uniform manipulating scheme. The basic idea of braiding is clear as shown in Fig. 1(b), in terms of manipulating the parameter vector \vec{R} . For a spin-1/2 particle in magnetic field, the vector in the parameter space just corresponds to the Bloch vector of the spin state, i.e., the eigenstate of $\sigma_n = \vec{\sigma} \cdot \vec{n}$, with \vec{n} the unit vector of \vec{R} . This would result in the well-known Berry phase characterized by the solid angle spanned to the closed trajectory in the parameter space. For the case of Majorana braiding as shown in Fig. 1(b), it will be more difficult to understand the similar result, despite that one can indeed obtain the same Berry phase by means of certain more sophisticated treatment [38,39].

Moreover, in order to handle the nonadiabatic effect during evolution along the parameter trajectory shown in Fig. 1(b), we would like to describe the state evolution using the occupation-number-state representation. In general, the state can be expressed as

$$|\Psi(t)\rangle = \alpha(t)|E_-(t)\rangle + \beta(t)|E_+(t)\rangle, \quad (3)$$

where $|E_-(t)\rangle$ and $|E_+(t)\rangle$ are the instantaneous eigenstates of the two-state system under study. In the adiabatic case, we always have $\beta(t) = 0$, since there is no nonadiabatic transition occurring. The system will always stay in the instantaneous eigenstate connected with the initial state, say, $|0_{23}0_d\rangle$ assumed here. We thus have $|\alpha(t)| = \alpha(0) = 1$. At the end of braiding, $\alpha(T) = e^{i\varphi}\alpha(0)$. The most important point is that the phase factor φ does not contain only the expected dynamical phase $\varphi_d = -\frac{1}{\hbar}\int_0^T dt E_-(t)$, but also a geometric phase φ_g , i.e., the Berry phase determined by the solid angle as shown

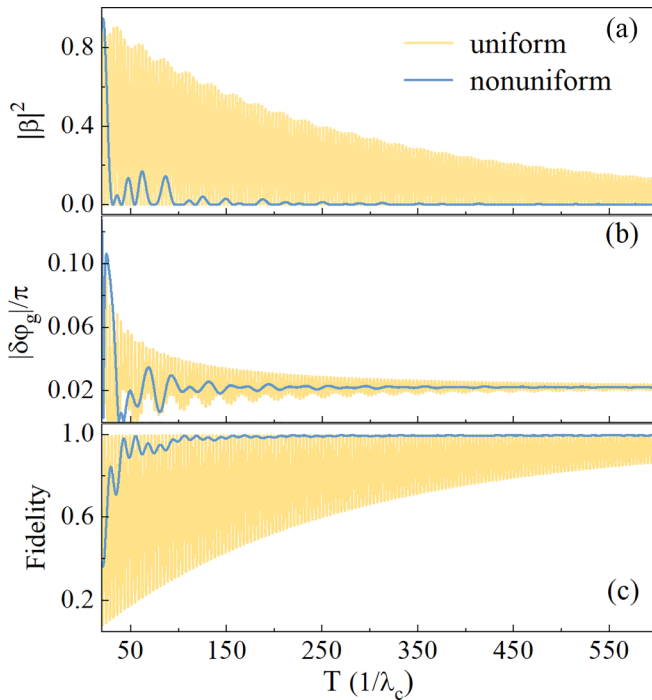


FIG. 2. Nonadiabatic effect of the four-step uniform (yellow lines) and nonuniform (blue lines) manipulation schemes, shown by the total braiding time dependence (a) for the transition probability, (b) for the geometric phase error from the Berry phase $-\pi/4$, and (c) for the fidelity of the four-MZM qubit state rotation. In all simulations of this work, arbitrary units of energy are assumed by setting the maximum coupling strength $\lambda_c = 1.0$. In this plot, the quantum dot energy level is assumed as $\varepsilon_d = 0.2\lambda_c$.

in Fig. 1(b). Therefore, in total, we have $\varphi = \varphi_d + \varphi_g$. In the presence of nonadiabatic transition, in addition to $\beta(t) \neq 0$, the remaining part from the phase $\varphi(T)$ after subtracting the dynamic phase $\varphi_d(T)$ will also deviate from the geometric phase φ_g determined by the solid angle spanned in the parameter space. We will show that both errors will affect the fidelity of the braiding operation.

In Fig. 2 we show the numerical results simulated based on the considerations outlined above. The scheme of four-step uniform modulation of the coupling strengths can be summarized as $|d\lambda_{1,2}/dt| = \frac{\lambda_c}{T/4}$, which are involved sequentially in the following modulations: (i) with $|\lambda_1|$ increased from zero to λ_c , (ii) with $|\lambda_2|$ increased from zero to λ_c , (iii) with $|\lambda_1|$ decreased from λ_c to zero, and (iv) with $|\lambda_2|$ decreased from λ_c to zero. In Figs. 2(a) and 2(b) we show the results of the nonadiabatic transition probability $|\beta|^2$ and the geometric phase error (deviated from the Berry phase $-\pi/4$), versus the braiding time T . In general, as expected, the nonadiabatic transition is less prominent with increase of T . The behavior of oscillations observed in Fig. 2(a) is owing to the Landau-Zener-Stückelberg (LZS) interference [43–45] between the (relatively strong) nonadiabatic transitions near $t = 0$ and $t = T$, where the energy gap is small. In Fig. 2(b), we find that the geometric phase extracted from the dynamic (nonadiabatic) evolution deviates also from the result of the adiabatic case, i.e., the geometric phase $\varphi_g = -\Omega_c/2$, while the solid angle

takes the value of $\Omega_c = \arcsin[4\lambda_c^2/(\varepsilon_d^2 + 4\lambda_c^2)]$, numerically which corresponds to the asymptotic result in the long- T limit in Fig. 2(b).

The two errors shown in Figs. 2(a) and 2(b) will affect the fidelity of the logic gate associated with the braiding operation. In an ideal case with no errors, the desired state of the four-MZM qubit after braiding is $|\psi_g\rangle$, as shown in Eq. (1). The fidelity compared with this state is given by $\mathcal{F} = \text{Tr}_M(|\psi_g\rangle\langle\psi_g|\rho_M)$, where $\rho_M = \text{Tr}_D[|\Psi(T)\rangle\langle\Psi(T)|]$ is the reduced density matrix after tracing out the QD degree of freedom from the total state $|\Psi(T)\rangle$; thus the remaining trace $\text{Tr}_M(\dots)$ is over the Majorana qubit states. In Fig. 2(c), we show the numerical result of the fidelity. We find that the fidelity is largely affected by the nonadiabatic transition probability $|\beta|^2$ shown in Fig. 2(a).

We know that the relatively strong nonadiabatic transitions largely take place near $t = 0$ and $t = T$, where the energy gap is small as shown in Fig. 1(c). Qualitatively speaking, in order to avoid strong nonadiabatic transition, one should modulate the parameter change more slowly for smaller energy difference $\Delta E = E_+ - E_-$. Therefore, let us consider a nonuniform change of the parameters in the four-step modulation scheme according to $|d\lambda_{1,2}/dt| = \eta(E_+ - E_-)^2/\hbar$, where the dimensionless parameter η is introduced to control the parameter modulation speed. If $\eta \ll 1$, the well-known adiabatic condition is satisfied. On the contrary, if $\eta > 1$, remarkable nonadiabatic transition will take place. For this nonuniform scheme of parameter modulation, it is possible to carry out an analytic expression for the total time of braiding. The individual times for each of the four steps can be obtained as

$$\begin{aligned} T_1 = T_4 &= \frac{1}{2\eta\varepsilon_d} \arctan \frac{2\lambda_c}{\varepsilon_d}, \\ T_2 = T_3 &= \frac{1}{2\eta\sqrt{\varepsilon_d^2 + 4\lambda_c^2}} \arctan \frac{2\lambda_c}{\sqrt{\varepsilon_d^2 + 4\lambda_c^2}}. \end{aligned} \quad (4)$$

The total braiding time is their sum, $T = T_1 + T_2 + T_3 + T_4$. From this, one can determine η from T , for given parameters ε_d and λ_c . In Figs. 2(a), 2(b), and 2(c) we plot also the results of the nonuniform modulation scheme, in close comparison with the results of the uniform scheme. We find that, remarkably, the nonadiabatic transition can be largely suppressed, with thus an important advantage of allowing much shorter braiding times.

In Fig. 3 we show further the particular effect of the dot energy ε_d . In Fig. 3(a), the dependence of the minimum braiding time T_m on the dot energy ε_d is shown for both the uniform and nonuniform modulation schemes. The minimum braiding time T_m is determined from the threshold value of the nonadiabatic transition probability $|\beta(T)|^2 < 0.1$ if $T > T_m$. Again, we find that the results of the nonuniform modulation scheme are much better than the uniform scheme. This becomes more prominent with decrease of the dot energy. In Fig. 3(b) we show the geometric phase versus the dot energy ε_d , where the results (symbols) extracted from the real-time dynamic evolution are plotted against the adiabatic value (blue line) determined by the solid angle as shown in Fig. 1(b).

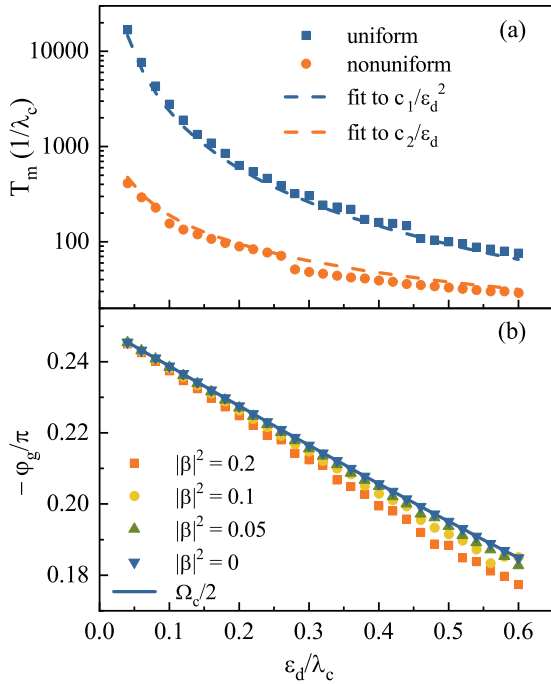


FIG. 3. (a) Minimum braiding time T_m under the condition $|\beta|^2 \leq 0.1$ versus the dot energy level ε_d , for the four-step uniform and nonuniform manipulation schemes. The numerical results are fitted by using c_1/ε_d^2 and c_2/ε_d , respectively, while $c_1 = 32 \ln 10/\pi$ is obtained through the formula of Landau-Zener transition probability and $c_2 \approx 19$ is obtained through numerical fitting. (b) Geometric phases (plotted by symbols) extracted from dynamic evolutions within the respective braiding time T_m under the specified threshold conditions. The blue line plots the analytic result of the Berry phase, $\Omega_c/2 = \frac{1}{2} \arcsin[4\lambda_c^2/(\varepsilon_d^2 + 4\lambda_c^2)]$.

IV. SIX-STEP SCHEME

In order to avoid strong nonadiabatic transitions near the beginning and end of the braiding operation, we need a relatively large dot energy, e.g., $\varepsilon_d = 2\lambda_c$. In order to achieve at the same time a complete braiding between γ_2 and γ_3 , which requires to realize an exact solid angle of $\Omega_c = \pi/2$ as schematically shown in Fig. 1(b), we further propose the following six-step modulation protocol: (i) with $|\lambda_1|$ increased from zero to λ_c , (ii) with ε_d decreased from $2\lambda_c$ to zero, (iii) with $|\lambda_2|$ increased from zero to λ_c , (iv) with $|\lambda_1|$ decreased from λ_c to zero, (v) with ε_d restored to the initial value from zero to $2\lambda_c$, and (vi) with $|\lambda_2|$ decreased from λ_c to zero. For each step, the modulation speed can be uniform, say, to modulate the energy with a constant rate.

In Fig. 4 we compare the results of this six-step scheme with the four-step protocol results shown in Fig. 2. As a more challenging comparison, we compare here only with the nonuniform four-step scheme, which has been demonstrated with better effect of suppressing the nonadiabatic transition. In Fig. 4(a), we find that the nonadiabatic transition can be largely suppressed even on a short timescale of braiding, while in Figs. 4(b) and 4(c) we find the precise geometric phase $\varphi_g = -\pi/4$ and good fidelity with the desired state $|\psi_g\rangle$ accomplished, which indicate a complete exchange of the MZMs γ_2 and γ_3 . Importantly, the uniform

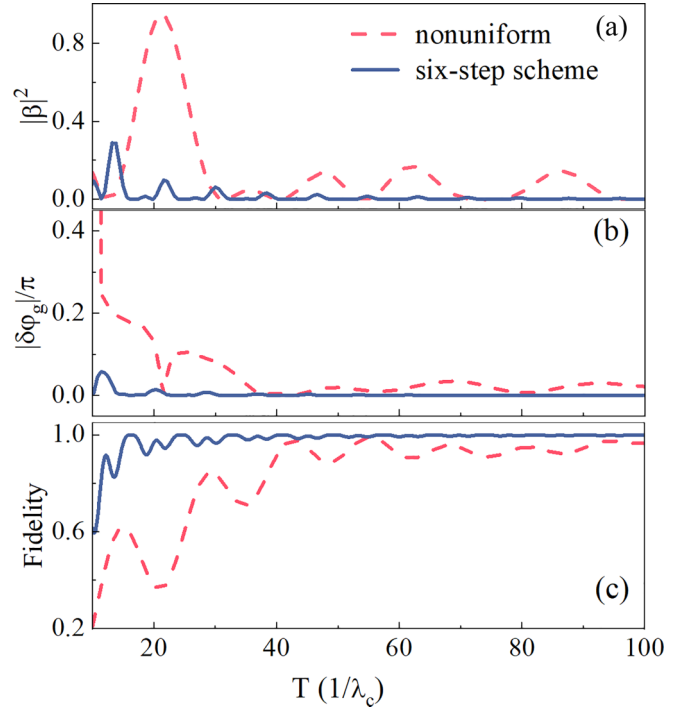


FIG. 4. Nonadiabatic effect of the improved six-step manipulation scheme, in comparison with the relatively good results of the four-step nonuniform scheme as shown in Fig. 2: Braiding time dependence plotted for (a) the transition probability, (b) the geometric phase error from $-\pi/4$, and (c) the fidelity of the four-MZM qubit state rotation. In the simulations, we assume $\varepsilon_d = 0.2\lambda_c$ in the whole process of the four-step manipulation, and $\varepsilon_d = 2\lambda_c$ as the initial and final values of the dot energy for the six-step scheme.

six-step modulation should be more feasible in practice than the adiabatic-condition-guided nonuniform four-step scheme analyzed above. Here, only an additional modulation of the dot energy ε_d is added. This can be done similarly as modulating the coupling strengths via electric gate control.

V. SHORTCUTS-TO-ADIABATICITY APPROACH

Finally, we notice that a popular method of suppressing the nonadiabatic transition is the so-called shortcuts-to-adiabaticity (STA) approach [46–49]. The basic idea of STA is to add auxiliary counterdiabatic driving so that the dynamics can follow the adiabatic evolution. For the two-state system under present study, as shown in Figs. 1(b) and 1(c), the counterdiabatic driving Hamiltonian can be obtained as $H'(t) = i\hbar(\zeta_1\gamma_B\gamma_3 + \zeta_2\gamma_B\gamma_2 + \zeta_3\gamma_2\gamma_3)/\Delta^2$, where $\Delta^2 = \varepsilon_d^2 + 4|\lambda_1|^2 + 4|\lambda_2|^2$, $\zeta_j = (-1)^j(|\lambda_j|\varepsilon_d - \dot{\varepsilon}_d|\lambda_j|)$ for ζ_1 and ζ_2 , and $\zeta_3 = 2(|\lambda_1\lambda_2| - |\dot{\lambda}_1\lambda_2|)$. Then, the total Hamiltonian to affect the system evolution is $H(t) = H_M(t) + \kappa H'(t)$. Here we introduce an overall strength parameter κ for the counterdiabatic driving, in order to demonstrate the effect of the STA approach. In Fig. 5 we display the effect of the STA counterdiabatic driving on the nonadiabatic transition probabilities for the uniform four-step, nonuniform four-step, and uniform six-step schemes in Figs. 5(a)–5(c), respectively, on different timescales based on the previous existing results. For each case, we consider the counterdiabatic driving strengths

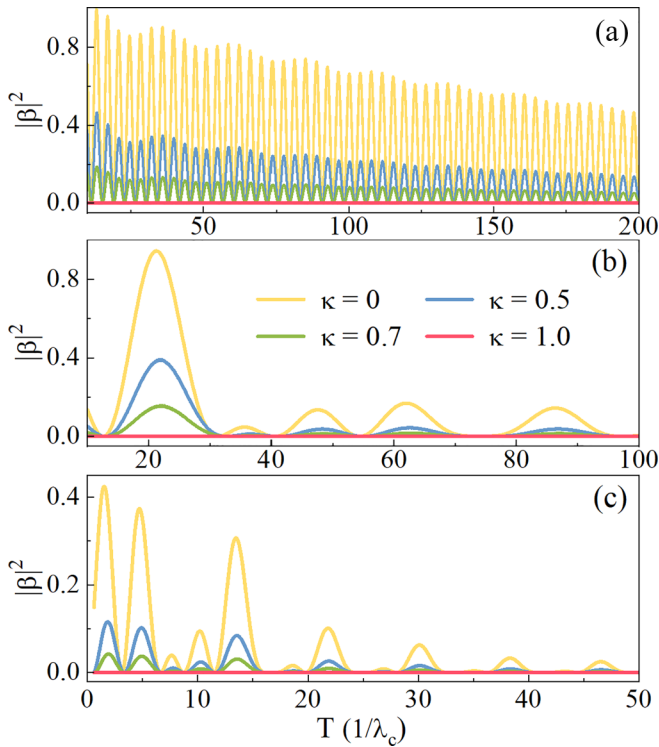


FIG. 5. Effect of counterdiabatic driving, by varying its action strength κ , based on the shortcuts-to-adiabaticity approach. Nonadiabatic transition probabilities for (a) the four-step uniform scheme, (b) the nonuniform scheme, and (c) the six-step manipulation scheme. The quantum dot energy level ε_d is assumed the same as explained in the caption of Fig. 4.

of $\kappa = 0, 0.5, 0.7$, and 1 . As expected, nonadiabatic transition can be suppressed for every case if we perform the full control with $\kappa = 1$. The results shown in Fig. 5 are indeed satisfactory. However, one can easily find that the counterdiabatic driving Hamiltonian is very hard to be realized in practice. Here, in addition to switching on coupling between γ_B and (γ_2, γ_3) , we also need to establish coupling between γ_2 and γ_3 . All these couplings are beyond the original manipulation couplings as shown in Fig. 1(b). Moreover, the most serious difficulty is that precise realization of these time-dependent coupling strengths is seemingly impossible in practice. Deviations from these mathematically designed coupling strengths will result in a failure to the success as roughly shown in Fig. 5.

VI. SUMMARY AND DISCUSSION

By simulating the real-time dynamics of braiding a pair of MZMs through a quantum dot, we revealed the strong nonadiabatic effect when the dot energy level approaches zero as required for a full exchange between the MZMs. We simulated and compared the results of different schemes. Rather than nonuniformly manipulating the system according to adiabatic conditions and the shortcuts-to-adiabaticity strategy, we proposed a simpler and more feasible scheme of six-step manipulations to suppress the nonadiabatic transition, which

allows as well for a full exchange between the Majorana modes.

The Majorana braiding protocol analyzed in this work (with the help of a quantum dot) is quite compatible with the nowadays hybrid semiconductor-superconductor experimental platforms. It is also the minimal 1D realization of braiding a pair of MZMs. We may highlight that the scheme of the six-step manipulations has obvious advantages over the nonuniform four-step scheme and the shortcuts-to-adiabaticity approach, since it should be very difficult in practice to implement the time-dependent precise controls required by the latter schemes. The nonadiabatic transitions can be inferred via the dot electron occupation, which can be further detected by a nearby charge-sensitive detector such as quantum-point-contact device. Moreover, the braiding resultant state, given by Eq. (1), and deviations from it, can be verified by moving (via gate-voltage controls) the Majorana modes γ_2 and γ_3 to the other ends of the wires, to fuse with γ_1 and γ_4 . Then, one can measure the occupations n_{12} and n_{34} of the fused regular fermions, by coupling them to individual quantum dots and quantum-point-contact detectors, following the proposal in Ref. [50] to initialize the Majorana pairs for demonstrating the nontrivial fusion of Majorana fermions. We believe that along this line, based on the platform of quantum-dot-coupled Majorana wires, demonstrating the non-Abelian statistics of MZMs should be an attractive research project.

Finally, we make a few remarks on issues not well discussed in the main text. During the braiding operation started with $|0_{12}0_{34}0_d\rangle$, there exist two evolution channels, which are associated with initial states $|0_{23}0_d\rangle$ and $|1_{23}0_d\rangle$, respectively. We have displayed detailed results of the former channel in the main text, but would like to briefly discuss the latter channel (with similar results) in Appendix A. Also, despite that in this work we consider tuning local couplings to realize braiding, the global geometric-phase-based scheme is not sensitive to inaccuracy of the parameter fine tunings, which actually falls into the scenario of geometric quantum computation (GQC) and holonomic quantum computation (HQC) [51–53], holding thus inherent stability against local perturbations. In this context, we may pay special attention to the possible inaccurate control of the phases $\phi_1 = \pi$ and $\phi_2 = 0$. The control errors $\delta\phi_1$ and $\delta\phi_2$ will cause couplings of γ_2 and γ_3 to γ_B [see Fig. 1(b)]. In Appendix B, we analyze this issue in detail and achieve conclusions as follows.

(i) A systematic deviation of the phase difference $\phi_1 - \phi_2$ from π will cause state fidelity error, as shown by Fig. 7 in Appendix B. Actually, the Berry phase (geometric solid angle) in GQC and HQC suffers also this type of problem.

(ii) If the phase difference $\phi_1 - \phi_2$ suffers certain fluctuations around the desired value π (this should be the most possible situation in a real system), the state error caused by the dynamic phase difference will be averaged out, making thus the result hold similar robust features of the geometric solid angle, as shown by Fig. 8 in Appendix B.

ACKNOWLEDGMENTS

This work was supported by the NNSF of China (Grants No. 11974011 and No. 11904261).

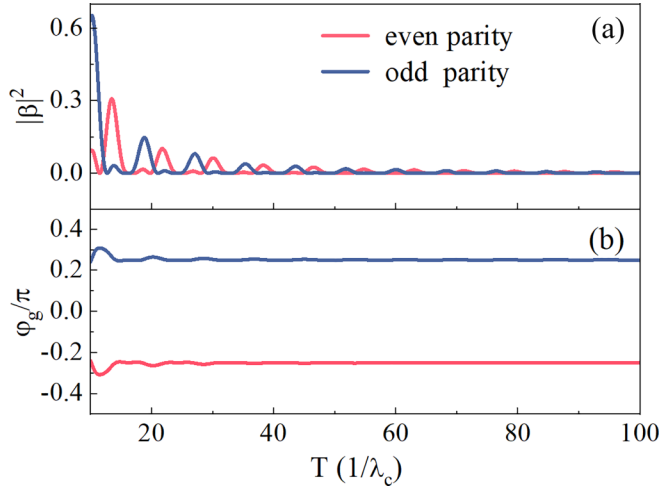


FIG. 6. Comparison of nonadiabatic effect between the two evolution channels associated with initial states $|0_{23}0_d\rangle$ and $|1_{23}0_d\rangle$, in the subspaces $\{|0_{23}0_d\rangle, |1_{23}1_d\rangle\}$ (even parity) and $\{|1_{23}0_d\rangle, |0_{23}1_d\rangle\}$ (odd parity), respectively. As a representative illustration, the optimal six-step scheme is exemplified in this simulation. Parameters and notations used here are the same as in Fig. 4.

APPENDIX A: NONADIABATIC TRANSITION EFFECT STARTING WITH $|1_{23}0_d\rangle$

The four-MZM setup is the minimal realization of a Majorana logic qubit (with fixed fermion parity). For instance, the even-parity logic qubit can be defined by the two basis states $|0\rangle_L = |0_{12}0_{34}\rangle$ and $|1\rangle_L = |1_{12}1_{34}\rangle$. As shown by Eq. (1) in the main text, after braiding γ_2 and γ_3 , the qubit state would experience a rotation, $|0_{12}0_{34}\rangle \rightarrow |\psi_g\rangle = \frac{1}{\sqrt{2}}(|0_{12}0_{34}\rangle - i|1_{12}1_{34}\rangle)$. In Figs. 2(c) and 4(c) for, respectively, the four-step and six-step manipulation schemes, we display the fidelity of the reduced state that suffered nonadiabatic transition with this target state. The numerical simulation was just performed using the basis states $|n_{12}n_{34}n_d\rangle$. We find that the fidelity is largely affected by the nonadiabatic transition probability $|\beta|^2$ as shown in Figs. 2(a) and 4(a).

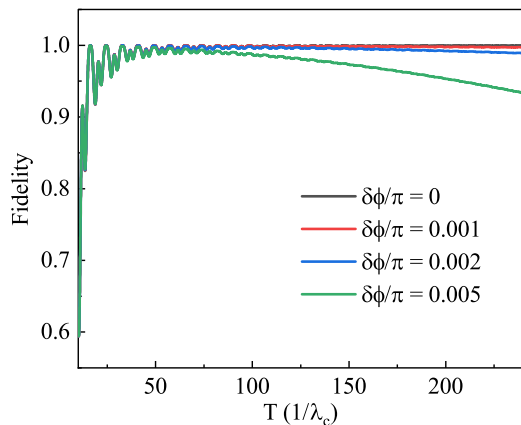


FIG. 7. Effect of small phase errors of the coupling amplitudes. It is found that the fidelity is more seriously affected by stronger phase error $\delta\phi$, especially with the increase of the braiding time T . Parameters used in this simulation are the same as in Fig. 4.

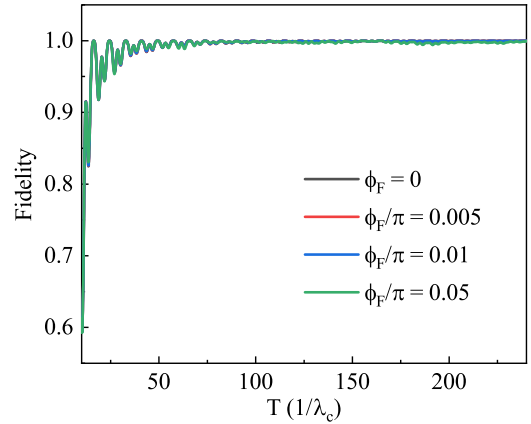


FIG. 8. State fidelity in the presence of fluctuations of the phase difference $\phi_1 - \phi_2$ around the required value π . $\delta\phi(t) = \phi_F \xi(t)$ is assumed in the simulation, while $\xi(t)$ is a homogeneous random number between $[-1, 1]$ for each time step of the state propagation. Other parameters used in the simulation are the same as in Fig. 4. Results for a few fluctuation strengths are shown.

During the braiding operation started with $|0_{12}0_{34}0_d\rangle$, actually there exist two evolution channels, which are associated with initial states $|0_{23}0_d\rangle$ and $|1_{23}0_d\rangle$, respectively. To see this, let us prove the following transformation rule:

$$|0_{12}0_{34}\rangle = \frac{1}{\sqrt{2}}(|0_{23}0_{14}\rangle - i|1_{23}1_{14}\rangle). \quad (\text{A1})$$

Under the constraint of fermion parity, in general, we may first construct the transformation ansatz as $|0_{12}0_{34}\rangle = a|0_{23}0_{14}\rangle + b|1_{23}1_{14}\rangle$. Then, we express the operator $f_{12} = \gamma_1 - i\gamma_2$ in terms of the regular fermion operators f_{14} and f_{23} as

$$f_{12} = \frac{1}{2}(f_{14} + f_{14}^\dagger - if_{23} - if_{23}^\dagger). \quad (\text{A2})$$

This result is obtained by simply associating the Majorana fermions γ_1 and γ_4 with the regular fermion f_{14} , and γ_2 and γ_3 with f_{23} , respectively. Thus we have $\gamma_1 = (f_{14} + f_{14}^\dagger)/2$ and $\gamma_2 = (f_{23} + f_{23}^\dagger)/2$. Furthermore, acting the annihilation operator f_{12} on both sides of the ansatz equation, we have

$$0 = \frac{a}{2}(|0_{23}1_{14}\rangle - i|1_{23}0_{14}\rangle) + \frac{b}{2}(-i|0_{23}1_{14}\rangle - |1_{23}0_{14}\rangle). \quad (\text{A3})$$

During the algebra, one should notice the difference of a minus sign between $f_{23}|1_{23}1_{14}\rangle = |0_{23}1_{14}\rangle$ and $f_{14}|1_{23}1_{14}\rangle = -|1_{23}0_{14}\rangle$. From this result, we obtain $a = ib = 1/\sqrt{2}$, which fulfills the proof of the above formula of transformation. Applying the same method outlined above, one can straightforwardly carry out all the transformation formulas between the two sets of basis states, $|n_{12}n_{34}\rangle$ and $|n_{23}n_{14}\rangle$.

Then, from the above Eq. (A1), we know that for the braiding operation started with $|0_{12}0_{34}0_d\rangle$, there are two channels of evolution. One starts with $|0_{23}0_d\rangle$, and another with $|1_{23}0_d\rangle$. In ideal case (without nonadiabatic transition), after the cyclic evolution, both states gain a geometric phase (with a difference of sign), i.e., $|0_{23}0_d\rangle \rightarrow e^{-i\pi/4}|0_{23}0_d\rangle$ and $|1_{23}0_d\rangle \rightarrow e^{i\pi/4}|1_{23}0_d\rangle$. This makes the state transformed back to the representation of $|n_{12}n_{34}\rangle$ become the target state $|\phi_g\rangle$. In the

presence of nonadiabatic transition, the resultant state (the reduced state ρ_M analyzed in the main text) deviates from $|\phi_g\rangle$, as characterized by the fidelity \mathcal{F} [see Figs. 2(c) and Fig. 4(c)].

Here, in Fig. 6, we numerically compare the nonadiabatic effects between the two evolution channels associated with initial states $|0_{23}0_d\rangle$ and $|1_{23}0_d\rangle$, in the subspaces $\{|0_{23}0_d\rangle, |1_{23}1_d\rangle\}$ (even parity) and $\{|1_{23}0_d\rangle, |0_{23}1_d\rangle\}$ (odd parity), respectively. As a representative illustration, we only present results from simulation of the six-step scheme. We find that the nonadiabatic transition in both channels can be suppressed in a similar way by properly increasing the braiding time T , as seen from $|\beta|^2 \rightarrow 0$ in Fig. 6(a). In Fig. 6(b), we find that the geometric phases acquired by $|0_{23}0_d\rangle$ and $|1_{23}0_d\rangle$ after the cyclic evolution are always the same in magnitude but differ in sign. However, for short braiding time T , the nonadiabatic transition probabilities in both channels do not coincide with each other. The reason is that for the evolution in each subspace, the instantaneous eigenstates are not the same, despite that the instantaneous eigenenergies are identical in the absence of coupling amplitude phase errors. For the effect of such errors, see Appendix B.

APPENDIX B: EFFECT OF SMALL PHASE ERRORS OF THE COUPLING AMPLITUDES

As explained in the main text, above Eq. (2) (for obtaining it), we assume $\phi_1 = \pi$ and $\phi_2 = 0$ (this can be realized by controlling the phases of the s -wave superconductors through magnetic fluxes (based on the Aharonov-Bohm effect) as explored in Refs. [40–42]). This choice allows the MZMs γ_2 and γ_3 coupled only with γ_A , but not with γ_B (after decomposing the dot electron into a pair of Majorana fermions), as shown in Fig. 1(b) for the basic idea of geometric approach to braid γ_2 and γ_3 .

Below we analyze the effect of small deviations $\delta\phi_1$ and $\delta\phi_2$. Better, let us introduce the relative phase error $\delta\phi = (\phi_1 - \phi_2) - \pi$. As to be clear soon, it is this relative phase error that will affect the result. One can check that the phase error $\delta\phi \neq 0$ will cause nonzero coupling of γ_2 and γ_3 to γ_B . Thus the solid-angle-based geometric analysis does not work. We thus present our analysis using the occupation-number-state representation. Based on the coupling Hamiltonians H'_1 and H'_2 , we can reexpress the coupling between (γ_2, γ_3) and the quantum dot as

$$\begin{aligned} H'_A &= \lambda_A d^\dagger f_{23}^\dagger + \text{H.c.}, \\ H'_N &= \lambda_N d^\dagger f_{23} + \text{H.c.} \end{aligned} \quad (\text{B1})$$

Here the regular fermion operator is defined as $f_{23} = \gamma_2 - i\gamma_3$. The former coupling Hamiltonian H'_A describes the Andreev process from Cooper pair splitting and recombination, and the latter H'_N describes the usual normal tunneling process. Here and in the following in this Appendix, we introduce indices ‘‘A’’ and ‘‘N’’ to distinguish the two processes. The coupling amplitudes of both processes are given by

$$\lambda_{A,N} = i(\lambda_1^* \pm \lambda_2^*) = i\lambda_1^* \left(1 \pm \frac{|\lambda_2|}{|\lambda_1|} e^{i(\phi_1 - \phi_2)/2}\right). \quad (\text{B2})$$

Now let us consider the braiding operation started with $|0_{12}0_{34}0_d\rangle$. From Eq. (A1) we know that there exist two

evolution channels associated with initial states $|0_{23}0_d\rangle$ and $|1_{23}0_d\rangle$, in the subspaces $\{|0_{23}0_d\rangle, |1_{23}1_d\rangle\}$ and $\{|1_{23}0_d\rangle, |0_{23}1_d\rangle\}$, respectively. The former is governed by the Andreev process, while the latter is governed by the normal tunneling process. In the limit of strictly adiabatic evolution, we have (after the cyclic evolution)

$$\begin{aligned} |0_{23}0_d\rangle &\longrightarrow e^{i\varphi_d^A + i\varphi_g^A} |0_{23}0_d\rangle, \\ |1_{23}0_d\rangle &\longrightarrow e^{i\varphi_d^N + i\varphi_g^N} |1_{23}0_d\rangle. \end{aligned} \quad (\text{B3})$$

The dynamic and geometric phases are given by

$$\begin{aligned} \varphi_g^{A,N} &= \mp \frac{\pi}{4} - \frac{\delta\phi}{4}, \\ \varphi_d^{A,N} &= -\frac{1}{\hbar} \int_0^T dt E_-^{A,N}(t). \end{aligned} \quad (\text{B4})$$

The interesting point revealed by this result is that the relative geometric phase (the difference of φ_g^A and φ_g^N) remains unchanged in the presence of the phase error ($\delta\phi \neq 0$), while the difference of the dynamic phases φ_d^A and φ_d^N is no longer zero when $\delta\phi \neq 0$, since the instantaneous eigenstate energies $E_\pm^A \neq E_\pm^N$ [refer to Fig. 1(c) for better understanding].

Based on Eqs. (A1) and (B3), owing to the phase difference between $|0_{23}0_{14}\rangle$ and $|1_{23}1_{14}\rangle$ accumulated during the cyclic evolution, we know that after transforming back to the basis states $|0_{12}0_{34}\rangle$ and $|1_{12}1_{34}\rangle$, the resultant state will be their superposition. If $\varphi_d^A = \varphi_d^N$, the result is just the target state $|\psi_g\rangle$ given by Eq. (1) in the main text, even after accounting for the change of the individual geometric phases (as shown above). However, if $\varphi_d^A \neq \varphi_d^N$, the resultant state will differ from $|\psi_g\rangle$, leading thus to the fidelity $\mathcal{F} < 1$.

In Fig. 7 we show the numerical results of fidelity $\mathcal{F} = \text{Tr}_M(|\psi_g\rangle\langle\psi_g|\rho_M)$, where the reduced density matrix ρ_M is obtained after tracing the quantum dot degree of freedom from the total state $|\Psi(T)\rangle$ associated with the six-step modulation scheme. In our simulation for the total state $|\Psi(t)\rangle$, we have accounted for nonadiabatic transition beyond adiabatic evolution. We find that, in agreement with the above analysis based on adiabatic evolution, the result is affected by the phase error $\delta\phi$, especially with increase of the total evolution time T . This implies that in practice, on one aspect, we should precisely control the coupling amplitude phases to make $\delta\phi \simeq 0$, and on the other aspect, we should shorten the braiding operation time T . From simulations for the several schemes carried out in this work, we conclude that the six-step protocol is the optimal choice.

The above analysis corresponds to a systematic deviation of the relative phase from $\phi_1 - \phi_2 = \pi$. Indeed, it will cause state fidelity error. However, for GQC and HQC, the Berry phase (geometric solid angle) suffers also this same problem. Actually, for GQC and HQC, the relatively robust nature is usually owing to the fact that the geometric solid angle is stable against possible fluctuations of parameters around their designed theoretical values of parameter control, based on an observation that the slightly fluctuating trajectory does not change the solid angle. Therefore, following the idea of stability analysis in GQC and HQC, we further consider the phase difference $\phi_1 - \phi_2$ suffering certain fluctuations around the desired value π (this should be the most possible situation

in a real system). From Eq. (B2), we find an interesting symmetry relation, $|\lambda_A(\delta\phi)|^2 = |\lambda_N(-\delta\phi)|^2$. Then, we anticipate that the state error caused by the dynamic phase difference $\varphi_d^A - \varphi_d^N$ will be averaged out, making thus the result hold similar robust features of the geometric solid angle. In Fig. 8,

we provide numerical support for this expectation. In the numerical simulation, we assume $\delta\phi(t) = \phi_F \xi(t)$, while $\xi(t)$ is a homogeneous random number between $[-1, 1]$ for each time step of the state propagation. We show results for a few fluctuation strengths in Fig. 8.

-
- [1] A. Y. Kitaev, Unpaired Majorana fermions in quantum wires, *Phys. Usp.* **44**, 131 (2001).
- [2] A. Y. Kitaev, Fault-tolerant quantum computation by anyons, *Ann. Phys.* **303**, 2 (2003).
- [3] C. Nayak, S. H. Simon, A. Stern, M. Freedman, and S. D. Sarma, Non-Abelian anyons and topological quantum computation, *Rev. Mod. Phys.* **80**, 1083 (2008).
- [4] B. M. Terhal, Quantum error correction for quantum memories, *Rev. Mod. Phys.* **87**, 307 (2015).
- [5] S. D. Sarma, M. Freedman, and C. Nayak, Majorana zero modes and topological quantum computation, *npj Quantum Inf.* **1**, 15001 (2015).
- [6] Y. Oreg and F. von Oppen, Majorana zero modes in networks of Cooper-pair boxes: Topologically ordered states and topological quantum computation, *Annu. Rev. Condens. Matter Phys.* **11**, 397 (2020).
- [7] V. Mourik, K. Zuo, S. M. Frolov, S. R. Plissard, E. P. A. M. Bakkers and L. P. Kouwenhoven, Signatures of Majorana fermions in hybrid superconductor-semiconductor nanowire devices, *Science* **336**, 1003 (2012).
- [8] S. M. Albrecht, A. P. Higginbotham, M. Madsen, F. Kuemmeth, T. S. Jespersen, J. Nygard P. Krogstrup and C. M. Marcus, Exponential protection of zero modes in Majorana islands, *Nature (London)* **531**, 206 (2016).
- [9] M. T. Deng, S. Vaitiekenas, E. B. Hansen, J. Danon, M. Leijnse, K. Flensberg, J. Nygard, P. Krogstrup and C. M. Marcus, Majorana bound state in a coupled quantum-dot hybrid nanowire system, *Science* **354**, 1557 (2016).
- [10] J. Alicea, Y. Oreg, G. Refael, F. von Oppen, and M. Fisher, Non-Abelian statistics and topological quantum information processing in 1D wire networks, *Nat. Phys.* **7**, 412 (2011).
- [11] B. I. Halperin, Y. Oreg, A. Stern, G. Refael, J. Alicea, and F. von Oppen, Adiabatic manipulations of Majorana fermions in a three-dimensional network of quantum wires, *Phys. Rev. B* **85**, 144501 (2012).
- [12] T. Karzig, G. Refael, and F. von Oppen, Boosting Majorana Zero Modes, *Phys. Rev. X* **3**, 041017 (2013).
- [13] M. Sekania, S. Plugge, M. Greiter, R. Thomale, and P. Schmitteckert, Braiding errors in interacting Majorana quantum wires, *Phys. Rev. B* **96**, 094307 (2017).
- [14] F. Harper, A. Pushp, and R. Roy, Majorana braiding in realistic nanowire Y-junctions and tuning forks, *Phys. Rev. Res.* **1**, 033207 (2019).
- [15] C. Tutschku, R. W. Reinthaler, C. Lei, A. H. MacDonald, and E. M. Hankiewicz, Majorana-based quantum computing in nanowire devices, *Phys. Rev. B* **102**, 125407 (2020).
- [16] L. Xu and X. Q. Li, Transport probe of the nonadiabatic transition caused by moving Majorana zero modes, *Phys. Rev. B* **105**, 245410 (2022).
- [17] D. J. Clarke, J. D. Sau, and S. Tewari, Majorana fermion exchange in quasi-one-dimensional networks, *Phys. Rev. B* **84**, 035120 (2011).
- [18] J. D. Sau, D. J. Clarke, and S. Tewari, Controlling non-Abelian statistics of Majorana fermions in semiconductor nanowires, *Phys. Rev. B* **84**, 094505 (2011).
- [19] C. S. Amorim, K. Ebihara, A. Yamakage, Y. Tanaka, and M. Sato, Majorana braiding dynamics in nanowires, *Phys. Rev. B* **91**, 174305 (2015).
- [20] S. Das Sarma, A. Nag, and J. D. Sau, How to infer non-Abelian statistics and topological visibility from tunneling conductance properties of realistic Majorana nanowires, *Phys. Rev. B* **94**, 035143 (2016).
- [21] B. van Heck, A. R. Akhmerov, F. Hassler, M. Burrello, and C. Beenakker, Coulomb-assisted braiding of Majorana fermions in a Josephson junction array, *New J. Phys.* **14**, 035019 (2012).
- [22] T. Hyart, B. Van Heck, I. Fulga, M. Burrello, A. Akhmerov, and C. Beenakker, Flux-controlled quantum computation with Majorana fermions, *Phys. Rev. B* **88**, 035121 (2013).
- [23] C. Knapp, M. Zaletel, D. E. Liu, M. Cheng, P. Bonderson, and C. Nayak, The Nature and Correction of Diabatic Errors in Anyon Braiding, *Phys. Rev. X* **6**, 041003 (2016).
- [24] C. K. McLauchlan and B. Béri, Fermion-Parity-Based Computation and Its Majorana-Zero-Mode Implementation, *Phys. Rev. Lett.* **128**, 180504 (2022).
- [25] K. Flensberg, Non-Abelian Operations on Majorana Fermions via Single-Charge Control, *Phys. Rev. Lett.* **106**, 090503 (2011).
- [26] C. Malciu, L. Mazza, and C. Mora, Braiding Majorana zero modes using quantum dots, *Phys. Rev. B* **98**, 165426 (2018).
- [27] S. Krøjer, R. S. Souto, and K. Flensberg, Demonstrating Majorana non-Abelian properties using fast adiabatic charge transfer, *Phys. Rev. B* **105**, 045425 (2022).
- [28] P. Bonderson, M. Freedman, and C. Nayak, Measurement-Only Topological Quantum Computation, *Phys. Rev. Lett.* **101**, 010501 (2008).
- [29] S. Hoffman, C. Schrade, J. Klinovaja, and D. Loss, Universal quantum computation with hybrid spin-Majorana qubits, *Phys. Rev. B* **94**, 045316 (2016).
- [30] T. Karzig, C. Knapp, R. M. Lutchyn, P. Bonderson, M. B. Hastings, C. Nayak, J. Alicea, K. Flensberg, S. Plugge, Y. Oreg, C. M. Marcus, and M. H. Freedman, Scalable designs for quasiparticle-poisoning-protected topological quantum computation with Majorana zero modes, *Phys. Rev. B* **95**, 235305 (2017).
- [31] S. Vijay and L. Fu, Teleportation-based quantum information processing with Majorana zero modes, *Phys. Rev. B* **94**, 235446 (2016).
- [32] V. Kornich, X. Huang, E. Repin, and Y. V. Nazarov, Braiding and All Quantum Operations with Majorana Modes in 1D, *Phys. Rev. Lett.* **126**, 117701 (2021).
- [33] D. J. Clarke, J. D. Sau, and S. Das Sarma, Probability and braiding statistics in Majorana nanowires, *Phys. Rev. B* **95**, 155451 (2017).

- [34] A. Rahmani, B. Seradjeh, and M. Franz, Optimal diabatic dynamics of Majorana-based quantum gates, *Phys. Rev. B* **96**, 075158 (2017).
- [35] Z. T. Zhang, F. Mei, X. G. Meng, B. L. Liang, and Z. S. Yang, Effects of decoherence on diabatic errors in Majorana braiding, *Phys. Rev. A* **100**, 012324 (2019).
- [36] A. Nag and J. D. Sau, Diabatic errors in Majorana braiding with bosonic bath, *Phys. Rev. B* **100**, 014511 (2019).
- [37] P. Marra, Majorana nanowires for topological quantum computation, *J. Appl. Phys.* **132**, 231101 (2022).
- [38] T. Karzig, Y. Oreg, G. Refael, and M. H. Freedman, Universal Geometric Path to a Robust Majorana Magic Gate, *Phys. Rev. X* **6**, 031019 (2016).
- [39] J. Liu, W. Chen, M. Gong, Y. Wu, and X. C. Xie, Minimal setup for non-Abelian braiding of Majorana zero modes, *Sci. China Phys. Mech. Astron.* **64**, 117811 (2021).
- [40] S. Hart, H. Ren, M. Kosowsky, G. Ben-Shach, P. Leubner, C. Brüne, H. Buhmann, L. Molenkamp, B. Halperin, and A. Yacoby, Controlled finite momentum pairing and spatially varying order parameter in proximitized HgTe quantum wells, *Nat. Phys.* **13**, 87 (2017).
- [41] H. Ren, F. Pientka, S. Hart, A. T. Pierce, M. Kosowsky, L. Lunczer, R. Schlereth, B. Scharf, E. M. Hankiewicz, L. W. Molenkamp, B. I. Halperin, and A. Yacoby, Topological superconductivity in a phase-controlled Josephson junction, *Nature (London)* **569**, 93 (2019).
- [42] B. Scharf, F. Pientka, H. Ren, A. Yacoby, and E. M. Hankiewicz, Tuning topological superconductivity in phase-controlled Josephson junctions with Rashba and Dresselhaus spin-orbit coupling, *Phys. Rev. B* **99**, 214503 (2019).
- [43] L. Landau, A theory of energy transfer, *Phys. Z. Sowjetunion* **2**, 46 (1932).
- [44] C. Zener, Non-adiabatic crossing of energy levels, *Proc. R. Soc. Lond. A* **137**, 696 (1932).
- [45] S. N. Shevchenko, S. Ashhab, and F. Nori, Landau-Zener-Stückelberg interferometry, *Phys. Rep.* **492**, 1 (2010).
- [46] M. Demirplak and S. A. Rice, Adiabatic population transfer with control fields, *J. Phys. Chem. A* **107**, 9937 (2003).
- [47] M. V. Berry, Transitionless quantum driving, *J. Phys. A: Math. Theor.* **42**, 365303 (2009).
- [48] T. Karzig, F. Pientka, G. Refael, and F. von Oppen, Shortcuts to non-Abelian braiding, *Phys. Rev. B* **91**, 201102(R) (2015).
- [49] K. Ritland and A. Rahmani, Optimal noise-canceling shortcuts to adiabaticity: Application to noisy Majorana-based gates, *New J. Phys.* **20**, 065005 (2018).
- [50] T. Zhou, M. C. Dartiailh, K. Sardashti, J. E. Han, A. Matos-Abiague, J. Shabani, and I. Zutic, Fusion of Majorana bound states with mini-gate control in two-dimensional systems, *Nat. Commun.* **13**, 1738 (2022).
- [51] P. Zanardi and M. Rasetti, Holonomic quantum computation, *Phys. Lett. A* **264**, 94 (1999).
- [52] L. M. Duan, J. I. Cirac, and P. Zoller, Geometric manipulation of trapped ions for quantum computation, *Science* **292**, 1695 (2001).
- [53] L. Cen, X. Q. Li, Y. J. Yan, H. Z. Zheng, and S. J. Wang, Evaluation of Holonomic Quantum Computation: Adiabatic Versus Nonadiabatic, *Phys. Rev. Lett.* **90**, 147902 (2003).